eNeuro

*Research Article: New Research | Disorders of the Nervous System*

# Whole-Brain Source-Reconstructed MEG-Data Reveal Reduced Long-Range Synchronization in Chronic Schizophrenia

## Reduced long-range synchronization in schizophrenia

**Jonni Hirvonen[1], Michael Wibral[2], J. Matias Palva[1], Wolf Singer[3,4,5], Peter Uhlhaas[6] and Satu Palva[1]**

[1]*Helsinki Institute of Life Sciences, Neuroscience Center, University of Helsinki, Finland*

[2]*MEG-Unit, Goethe-University, Frankfurt, Germany*

[3]*Department of Neurophysiology, Max Planck Institute for Brain Research, Frankfurt Am Main, Germany*

[4]*Ernst Strüngmann Institute for Neuroscience (ESI) in Cooperation with Max Planck Society, Frankfurt Am Main, Germany*

[5]*Frankfurt Institute for Advanced Studies (FIAS), Frankfurt Am Main, Germany*

[6]*Institute of Neuroscience and Psychology, University of Glasgow, Glasgow, UK*

DOI: 10.1523/ENEURO.0338-17.2017

Received: 2 October 2017

Accepted: 2 October 2017

Published: 9 October 2017

**Author Contributions:** JMP, SP, WS, PU, MW designed the research, JH analyzed data, JH, JMP, SP,WS, PU, MW wrote the paper.

**Funding:** http://doi.org/10.13039/501100005878Academy of Finland | Terveyden Tutkimuksen Toimikunta (Forskningsrådet för Hälsa)
267030
266402
273807
253130
256472

**Funding:** Research Foundation of the University of Helsinki

**Funding:** http://doi.org/10.13039/501100006306Sigrid Juséliuksen Säätiö (Sigrid Jusélius Stiftelse)

**Funding:** Lilly and Lundbeck

**Dr. Uhlhaas has received research support from Lilly and Lundbeck.**

P.U. and S.P. These authors contributed equally to this work.

**Correspondence should be addressed to** Satu Palva, Helsinki Institute of Life Sciences, Neuroscience Center, University of Helsinki, Finland. Phone: +358504484742, email: satu.palva@helsinki.fi

**Cite as:** eNeuro 2017; 10.1523/ENEURO.0338-17.2017

# Whole-Brain Source-Reconstructed MEG-Data Reveal Reduced Long-Range Synchronization in Chronic Schizophrenia

Abbreviated title: Reduced long-range synchronization in schizophrenia

Jonni Hirvonen[1], Michael Wibral[2], J. Matias Palva[1], Wolf Singer[3-5], Peter Uhlhaas[6*], and Satu Palva[1*]

[1] Helsinki Institute of Life Sciences, Neuroscience Center, University of Helsinki, Finland
[2] MEG-Unit, Goethe-University, Frankfurt, Germany
[3] Department of Neurophysiology, Max Planck Institute for Brain Research, Frankfurt am Main, Germany
[4] Ernst Strüngmann Institute for Neuroscience (ESI) in Cooperation with Max Planck Society, Frankfurt am Main, Germany
[5] Frankfurt Institute for Advanced Studies (FIAS), Frankfurt am Main, Germany.
[6] Institute of Neuroscience and Psychology, University of Glasgow, Glasgow, UK

* These authors contributed equally to this work.

**Corresponding author:** Satu Palva, Helsinki Institute of Life Sciences, Neuroscience Center, University of Helsinki, Finland. Phone:+358504484742, email:satu.palva@helsinki.fi

**Author Contributions**: JMP, SP, WS, PU, MW designed the research, JH analyzed data, JH, JMP, SP,WS, PU, MW wrote the paper.

**Funding:** This work was supported by the University of Helsinki Research Grants, Academy of Finland (SA 267030, SA 266402 and SA 273807 to SP and SA 253130 and 256472 MP), Research Foundation of the University of Helsinki to SP and JH, and Sigrid Juselius Foundation to SP and MP for supporting this study.

**Conflict of Interest Disclosure**

Dr. Uhlhaas has received research support from Lilly and Lundbeck

## Acknowledgements

We thank Christine Gruetzner for help in the acquisition of MEG/MRI-data.

Number of pages: 34
Number of figures: 7, Number of tables: 1
Number of words for Abstract: 2034
Number of words for Introduction: 666
Number of words for Discussion: 1072

## Abstract

**Current theories of schizophrenia posit that the symptoms and cognitive dysfunctions arise from a dysconnection syndrome. However, studies that have examined this hypothesis with physiological data at realistic time-scales are so far scarce. The current study employed a state-of-the-art approach using Magnetoencephalography (MEG) to test alterations in large-scale phase synchronization in a sample of *n* = 16 chronic schizophrenia patients, 10 males and *n* = 19 healthy participants, 10 males, during a perceptual closure task. We identified large-scale networks from source reconstructed MEG data using data-driven analyses of neuronal synchronization. Oscillation amplitudes and inter-areal phase-synchronization in the 3–120 Hz frequency range were estimated for 400 cortical parcels and correlated with clinical symptoms and neuropsychological scores. Schizophrenia patients were characterized by a reduction in gamma-band (30–120 Hz) oscillation amplitudes that was accompanied by a pronounced deficit in large-scale synchronization at gamma-band frequencies. Synchronization was reduced within visual regions as well as between visual and frontal cortex and the reduction of synchronization correlated with elevated clinical disorganization. Accordingly, these data highlight that schizophrenia is associated with a profound disruption of transient synchronization, providing critical support for the notion that core aspect of the pathophysiology arises from an impairment in coordination of distributed neural activity.**

## Significance statement:

Despite over 100 years of research, the pathophysiology of schizophrenia has remained elusive. Synchronization of neuronal activity across brain regions, a form of functional connectivity, is crucial for normal brain functioning. We tested the hypothesis that disruption of connectivity and synchronization could lead to the cognitive deficits in schizophrenia by recording magnetoencephalography (MEG) during a visual perceptual closure task. Long-range high-frequency synchronization in beta and gamma bands was reduced in chronic schizophrenic patients compared to healthy controls. This reduction of neuronal synchronization showed close correlations with the severity of clinical signs of cognitive disorganization. Reduced synchronization may thus constitute a core pathophysiological mechanism in schizophrenia.

## Introduction

Despite over 100 years of research, the pathophysiology of schizophrenia (ScZ) remains elusive. Previous theoretical and empirical frameworks explain the disorder as circumscribed alterations in neural circuits (Weinberger et al., 1988). An alternative hypothesis suggests that core aspects of symptoms and associated cognitive disturbances arise from a deficit in the functional integration of distributed brain networks leading to a dysconnection syndrome (Stephan et al., 2009). This hypothesis is supported by extensive evidence from normal brain functioning, suggesting that functional interactions between distributed neuronal ensembles are critical for the generation of coherent action and cognition (Singer, 1999; Varela et al., 2001). One mechanism to achieve such interactions is the synchronization of rhythmic activity that could promote effective coordination of neuronal processing (Fries, 2015; Gregoriou et al., 2009; Singer, 2009).

Given the crucial role of synchronization for effective brain functioning, one possibility is that a disruption in this process leads to behavioral and cognitive deficits observed in ScZ (Uhlhaas and Singer, 2015). Evidence from electro- and magnetoencephalography (EEG/MEG) has provided support for the possibility that both the amplitude of high-frequency oscillations and their long-range synchronization in relationship to perceptual processing are impaired (see Uhlhaas, 2015)). Several previous studies on perceptual integration have focused on the possibility that local neuronal synchronization, reflected by the amplitude/power of oscillatory activity, may be reduced at beta (14–30 Hz) and gamma-band frequencies along different stages of the visual hierarchy (Grent-'t-Jong et al., 2016; Grutzner et al., 2013; Spencer et al., 2003; Spencer et al., 2008; Uhlhaas et al., 2006;). Moreover, preliminary data also suggest abnormalities in long-range synchronization during perceptual integration (Spencer et al., 2003; Uhlhaas et al., 2006). These lines of research are consistent with evidence that synchronization of high-frequency oscillations may be associated with construction of coherent object representations during normal brain functioning (Grutzner et al., 2010; Keil et al., 1999; Rodriguez et al., 1999), and that disturbance in gamma-band synchronization may be at the root of the pervasive perceptual deficits in ScZ (Uhlhaas and Mishara, 2007; Uhlhaas and Singer, 2015).

A key limitation of most prior studies in ScZ is that estimates of neuronal synchronization were derived from scalp-EEG data. Because of volume conduction, individual EEG electrodes pick up signals from multiple neuronal and non-neuronal sources, such as muscles, which can give rise to artifacts and spurious correlations that yield false positives and mask true neuronal interactions (Brookes et al., 2012; Nolte et al., 2004; Palva and Palva, 2012; Schoffelen and Gross, 2009). These effects can be alleviated by using MEG data together with source reconstruction and synchronization metrics that are less sensitive to signal contamination and volume conduction (Palva and Palva, 2012; Schoffelen and Gross, 2009). Because of these methodological limitations, it is also currently unclear at which spatial scale and between which brain regions the

synchronization deficits occur in ScZ, *i.e.*, whether the putative anomalies are restricted to local cortical areas or involve also large-scale inter-areal neuronal interactions.

To overcome these limitations, we analyzed large-scale synchronization in a group of chronic ScZ-patients using MEG and applied a data-driven, whole-brain analysis of MEG-activity (Palva and Palva, 2012) obtained during a perceptual closure task. The data presented here were previously analyzed for MEG-sensor-level changes in beta/gamma-band power (Grutzner et al., 2013). MEG has an advantage over EEG in having a greater signal-to-noise ratio for high-frequency oscillations (Muthukumaraswamy and Singh, 2013) and better spatial resolution for localizing the underlying generators (Dale A and Sereno M, 1993; Sharon et al., 2007). Large-scale networks of neuronal synchronization were estimated among all parcels (brain areas) using source-modeled MEG. Parcellated data were then tested for modulations in within-parcel spectral power and inter-parcel phase-synchronization in the 3–120 Hz frequency range that was correlated with clinical symptoms and neuropsychological scores. We found that the ScZ-patients were characterized by a reduction in gamma-band amplitude (30–40 and 60–120 Hz) that was accompanied by a pronounced deficit in large-scale synchronization at beta/gamma-band frequencies. These abnormalities showed close correlations with the severity of clinical signs of cognitive disorganization.

## Material and methods

An overview of the MEG-analysis pipeline is given in Fig. 1. All data analyses, where not indicated otherwise, were performed on a LabVIEW-based (National Instruments) neuroinformatics platform that is available on request.

*Subjects and recordings*

We recruited 18 medicated ScZ-patients who met the DSM-IV criteria for ScZ from the Department of Psychiatry, Johann Wolfgang Goethe University, Frankfurt; Germany. Two patients had to be excluded because of missing channel data, leaving 16 patients (10 males, 3 left handed, mean age 37.06 ± 9.8). We also recruited 19 age- and gender-matched healthy control subjects (13 males, 4 left handed, mean age 32.42 ± 10.6) from the local community. All patients were on atypical neuroleptics at the time of testing. DSM-IV diagnosis for ScZ was confirmed by a trained psychologist with the SCID-interview for DSM-IV-R (First 1995). All ScZ-patients were on stable neuroleptic medication. Exclusion criteria were for both ScZ-patients and controls: (1) a neurological disorder, (2) alcohol, nicotine, or substance dependence within the last month, or (3) structural abnormalities in the T1 MR image. After having received a complete description of the study, each participant provided written informed consent. The study was approved by the ethical committee of the Goethe University Frankfurt.

Current psychopathology was assessed with the Positive and Negative Syndrome Scale (PANSS; (Kay et al., 1987) and symptoms were grouped into five factors according to the model of (Lindenmayer et al., 1995), including the factors “positive,” “negative,” “depression,” “excitement,” and “cognitive.” Cognitive function in patients and controls was measured with the Brief Assessment of Cognition in Schizophrenia (BACS) (Keefe et al., 2004) (Table 1).

MEG data were recorded continuously using a 275-channel whole-head system (Omega 2005, VSM MedTech Ltd., BC, Canada) at a rate of 600 Hz in a synthetic third order axial gradiometer configuration (Data Acquisition Software Version 5.4.0, VSM MedTech Ltd., BC, Canada). The data were filtered with 4th order butterworth filters with 0.5 Hz high-pass and 150 Hz low-pass. Behavioral responses were recorded using a fiber-optic response pad (Lumitouch, Photon Control Inc., Burnaby, BC, Canada) on the stimulus PC and fed through to the MEG acquisition system as an additional channel. Before and after each run, the subject’s head position relative to the

gradiometer array was measured using coils placed at the subject's nasion, and 1 cm anterior to the tragus of the left and right ear. Runs with total head displacement exceeding 5 mm were discarded.

*Anatomical (MRI) data acquisition*

A high-resolution anatomical MRI scan was acquired for each participant using a 3D magnetization-prepared rapid-acquisition gradient echo sequence (160 slices; voxel size: 1×1×1 mm; FOV: 256 mm; TR: 2300 ms; TE: 3.93 ms). During the structural scan, vitamin E pills were applied to the nasion and 1 cm anterior to the tragus of the right and left ear to allow for co-registration of the MEG and MRI data. Scanning was performed with a 3 tesla Siemens Trio scanner.

*Experimental protocol*

We used data from our previous study in which experimental procedures have been described (Grutzner et al., 2013). In brief, we presented a set of 160 Mooney faces (Mooney and Ferguson, 1951) , consisting of the 40 original Mooney stimuli presented in the upright orientation, mirrored at the vertical axis and in corresponding versions mirrored at the horizontal axis. Participants were presented with a random sequence of upright and inverted-scrambled stimuli which were shown for 200 ms (Fig. 2A). The inter-stimulus interval (ISI) ranged between 3500 and 4500 ms. Participants were required to indicate whether they detected a face or not via button press after each stimulus. They were instructed to respond as quickly as possible and to fixate a central fixation cross during the ISI. All participants completed four experimental runs, each of which was composed of 60 upright and 30 inverted scrambled stimuli. The stimuli were displayed in the center of a translucent screen at a viewing distance of 53 cm and subtended 19◦ of visual angle.

*Behavioral performance*

Hit rate (HR) was estimated as the proportion of correct responses from all responses to upright and inverted-scrambled Mooney-face stimuli. The correct responses were "No face" for inverted-scrambled Mooney faces and "Face" for upright stimuli. The latency at which either "Face" or "No face"-button was pressed was defined as the reaction time (RT).

*MEG data preprocessing, filtering, source analysis and surface parcellation*

Extra-cranial noise from the raw MEG recordings was removed with the temporal signal space separation method (tSSS) (Taulu et al., 2005) and independent component analysis (ICA) (Bell and Sejnowski, 1995) was used to identify and exclude components associated with eyes movements/blinks and cardiac artifacts (Fig. 1A). The preprocessed MEG time-series data from each separate channel was then narrow-band filtered into 31 frequency bands, $f_{min}$ = 3 Hz ... $f_{max}$ = 120 Hz by convolving the sampled MEG signals with a family of Morlet wavelets with $m$ = 5 (Fig. 1B). Finite impulse-response filter was used for broad-band filtering from 0.1 to 45 Hz (pass-band from 1 to 40 Hz) and Hilbert-transformation to obtain the signal phase time series (Palva et al., 2013) for the evoked responses (Fig. 4A).

We used FreeSurfer software (*http://surfer.nmr.mgh.harvard.edu/*) for automatic volumetric segmentation of the MRI data, surface reconstruction, flattening, cortical parcellation, and labeling with the Freesurfer/Destrieux atlas (Dale et al., 2000; Destrieux et al., 2010; Lin et al., 2006). MNE software (*http://www.nmr.mgh.harvard.edu/martinos/userInfo/data/sofMNE.php*) was used to create three-layer boundary element models (BEM), cortically constrained source models, MEG-MRI co-localization and for the preparation of the forward model and inverse operators (Gramfort et al., 2014; Hamalainen and Ilmoniemi, 1994). The source models had dipole orientations fixed to

the pial surface normals and a 7 mm source-to-source separation throughout the cortex yielding 6000 to 8000 source vertices. To reconstruct ongoing cortical dynamics, we used minimum-norm estimate (MNE) inverse operators in the form of dynamic statistical parametric maps (dSPM) (Dale et al., 2000) by computing noise-covariance matrices from the baseline (0.5 - 0.1 sec prior to stimulus onset) and using 0.05 as the regularization constant (Fig. 1C-D). The source time-series were collapsed to time series of 400 cortical parcels with a fidelity optimized collapse operator (Korhonen et al., 2014) from a precursor atlas of 148 parcels (Destrieux et al., 2010) by iteratively splitting the largest parcels of the Destrieux atlas along their most elongated axis using the same parcel-wise splits for all subjects (Fig. 1E).

*Analysis of oscillation amplitudes, evoked responses and inter-areal phase synchrony*

The collapsed parcel-wise narrow-band inverse estimates, $X_{F,P,r}(t,f)$ of single trials $r$, $r = 1\ldots n_s$, were used for cortex-wide mapping of evoked responses (Fig. 1G), induced amplitude modulations, and inter-areal phase synchronization (Fig. 1F). The averaged event-related amplitude envelopes were estimated separately for each trial type (upright correct, inverted correct, upright incorrect, inverted incorrect), cortical parcel, and wavelet frequency (Palva et al., 2005; Tallon-Baudry et al., 1996). The filtered evoked responses were obtained by the averaging the real parts of the complex filtered parcel time series.

Phase synchrony was estimated in 100 ms time-windows with 50 ms overlap separately for the same trial types as above for all frequencies and for all parcel pairs using the imaginary part of complex form of PLV (*iPLV*) to maximally attenuate artificial interactions caused by linear signal mixing, (Vinck et al., 2011). Since iPLV is sensitive to the number of trials, the trial number was balanced separately for each subject and for each contrast before the analyses by iteratively removing trials from the condition with more trials to match the condition with fewer trials s (Fig 1F). On average, 184 ± 38 (mean ± SD) and 104 ± 25 trials were obtained for the ScZ patients with

correctly perceived upright and inverted-scrambled stimuli, respectively. The control group had 234 ±57 and 126 ± 38 trials in upright and inverted-scrambled conditions, respectively.

To distinguish between synchronization caused by stimulus onset (evoked synchrony) and the dynamically generated synchronisation/phase locking (stimulus induced synchrony), we created trial-shuffled surrogate data for shift–predictor like estimation of stimulus-driven synchronization. However, in addition to eliminating non-stimulus-locked synchronization (Lachaux et al., 1999), trial-shuffling alone also eliminates the signal-mixing caused artificial couplings. In order to reconstruct the effects of signal mixing at MEG acquisition and the residual signal leakage after inverse modeling, we applied a novel forward-inverse-modeling based approach. This method eliminates confounds caused by the spatial spread of signals inherent in MEG/EEG recordings and reconstructs the signals preserving local source topography, amplitude dynamics and auto-correlation structures (Palva and Palva, 2012). This new approach permits more accurate identification of ”true” induced inter-areal interactions in the presence of signal mixing than the conventional trial shuffling procedure (Lachaux et al., 1999) that eliminates also the contributions of volume conduction and other signal mixing. We first used shuffled trials of source-modeled single-trial data in the 400-parcel time series for forward modeling, so that each source vertex of a parcel was simulated with this time series, and then source reconstructed these sensor-level surrogate data with procedures identical to those used for real data (Fig. 1H). Phase correlation analyses were then applied to these surrogate source data in the same way as to the real data for 10 independent realizations of the surrogate data. The means of surrogate data were subtracted directly from the corresponding real data in Figs. 4-7 (Fig. 1K).

*Statistical analyses and visualization (of the most significant effects)*

We used statistical testing across all brain regions, frequency bands, and time windows to reveal the task-related amplitude and synchrony modulation. Before performing statistical group analyses for

amplitude, individual data were baseline corrected parcel-by-parcel by subtracting from all samples the mean amplitude of a baseline period from 0.5 to 0.1 s prior to the stimulus onset. For the synchrony analyses, the iPLV values of the baseline time window at 0.225–0.125 s prior to stimulus onset were used for baseline correction. Significant differences between the responses to upright/inverted stimuli and the baseline period as well as between the upright and inverted stimuli were estimated with the Wilcoxon signed-rank test ($p < 0.05$). For the between-group comparisons, the Welch *t*-test was used separately for the Upright and Inverted conditions (Fig. 1i). In all analyses, only trials with correct responses were used. To reduce the false discovery rate (FDR) for each contrast, we pooled significant observations across all samples, frequency bands and cortical parcels and then discarded as many least-significant observations as were predicted to be false discoveries by the alpha-level used in the corresponding test (Rouhinen et al., 2013; Siebenhuhner et al., 2016).

To obtain a data-driven overview of all significant observations, we plotted for the amplitude data the fractions of parcels out of all 400 parcels exhibiting a statistically significant positive or negative effect ($P^{+}_{P}$ or $P^{-}_{P}$) for each time-frequency (TF) element in the peri-event TF plane. Likewise, to assess the extent of large-scale synchronization in each frequency band and time window, we defined connection density $K$ to be the fraction of significant edges of all possible edges ($K = k / (N-1)N$, where $k$ is the number of significant edges and $N$ is the number of parcels, $N = 400$). Similarly to the amplitudes, the connection densities were visualized in the TF plane. Graph theory (Bullmore and Sporns, 2009) was then used to characterize the networks formed by statistically significant parcel-parcel phase synchrony. Here, parcels constitute the nodes and significant synchronization the edges of the network.

*Visualization of the topography of amplitudes and network synchrony*

To identify the brain with the most prominent effects in the time- or time-frequency window-of-interest (TFROI), we displayed the fraction of significant TF-elements of all elements for each anatomical parcel, visualized on a representative inflated cortical surface ($P^{+}_{TF}/P^{-}_{TF}$) (Fig. 1J). Functional intrinsic network borders based on population level fMRI resting state activity (Yeo et al., 2011) were overlaid on the inflated surface as land marks.

Visualization of network synchrony is confounded due the linear signal mixing caused by inaccurate source reconstruction. We employed several new approaches to overcome this issue. We first assessed the reliability of source reconstructions and estimated interactions (Korhonen et al., 2014) and subsequently, to decrease the probability of reporting artificial and spurious synchronization, we removed from the subsequent analyses parcels with source reconstruction accuracy (fidelity) lower than 0.11. Next, we also excluded parcels that were prone to include oculomotor artefacts in MEG. The removed parcels were mostly located in orbital frontal, anterior and inferior temporal and medial structures (Fig. 1L).

Linear signal mixing also introduces artificial and spurious correlations into pairwise metrics of sensor or reconstructed source MEG data (Palva and Palva, 2012). Although iPLV is insensitive to zero- and π-phase lag coupling, it is sensitive to spurious interactions, *i.e.*, false positive connections arising from the signal mixing with neighbor of parcels with a true phase-lagged connection. Here we used a novel edge-bundling approach to group edges into bundles by their functional adjacency in linear mixing space so that the goal for bundling is to hierarchically cluster connections into groups that collectively reflect the true connections (Siebenhuhner et al., 2016). Such edge bundling results in a simplified and more appreciable graph with more reliable estimation of true edges and graph properties (Fig. 1O). For visualization, the resulting graphs (Figs. 5, 6) were co-localized with the seven functional brain systems of the Yeo parcellations (Yeo et al., 2011) (Fig. 1P).

*Estimation of synchronization patterns across different distances*

We computed normalized Euclidean distances for each pair of cortical parcels to assess the anatomical distance distribution of observed synchronization in the time-frequency-windows of interest. We selected the synchronization distances for each significant parcel pair from the average cortical distance-map based on the population mean of all the subjects in the study ($n$ = 35). Distance map comprised all the Euclidean distances derived from the RAS-space for each possible combination of 400 parcels yielding in total 160 000 distance values**.** These values were normalized by the longest possible distance on the whole cortex and the normalized Euclidean distances were binned into five bins. We then estimated the distances for the significantly synchronized parcel-pairs and the proportion of synchronization in each bin. These data was compared against a surrogate distance distribution that was built by randomly taking 5000 times the same number of edges and its 95 % -confidence intervals (Fig. 1S).

*Correlation with Clinical Symptoms*

To explore the putative links between inter-areal phase synchrony and clinical scores, we tested whether graph strength (GS) in the mid-gamma (40–51 Hz) band response co-varied with PANSS-ratings. To estimate individual *GS* values, we first computed individual weighted graphs by multiplying individual baseline corrected iPLV interaction matrices with a binary mask based on group graphs, *M(Group)*. Parcels and edges removed for low reconstruction accuracy or at-risk for oculomotor artifacts were excluded by masking (*M(DEM)*) from this analysis as well. Binary masks were defined for the mid-gamma (40–51 Hz) band and 125–325 ms time-window for the contrast of upright- vs. inverted Mooney stimuli and controls - ScZ (Fig. 6B). If the interaction at frequency $f$ and in time window $t$ was found significant between parcels $p$ and $q$ in the group-level analysis, $M(p, q, m, t, f)$ was set to 1, otherwise to 0. For each subject, we multiplied adjacency matrices with these masks and then summed over all parcel pairs. Subjects' individual *GS* for the time and frequency

window of interest was thus calculated as: $GS = \sum_{i=t,f}^{N}(M(Group)_i * M(DEM)_i * S_i)$,where M(x) are binary masks as defined above and S synchronization strength in the given time- (*t*) and frequency-window (*f*) for total of N windows. *GS* values were then sorted according to clinical scores and plotted as a function of increasing scores. Pearson correlation was used to estimate the correlation and bootstrapping with 10000 surrogates to estimate confidence limits (Fig. 1R).

*Summary of statistical analyses*

All statistical analyses are described in detail in respective positions of the Method section and summarized here. Primary statistical analyses between conditions were performed either with two-sample t-test, or Welch-t test of analysis of covariance for all time-windows and frequencies. To correct for multiple comparisons, we discarded the number of least significant observations that was predicted by the alpha-level and visualized only the observations that were above this threshold (Figures 3a, 4a, 6b). The exact p-values in the TFRs are not reported because of the large number of individual observations. To minimize the number of false positive connections (Figures 5 and 6c), we used several novel approaches. We first removed from the subsequent analyses the parcels with low source reconstruction accuracy or parcels that were prone to detect oculomotor artefacts. We then used a novel edge-bundling approach to group edges into bundles by their adjacency in the linear mixing space, which both inherently reduces the fraction of false positives and illustrates the most likely and statistically robust true neuronal connections.

## Results

*Behavioral performance*

In the control group, Hit Rate (HR) for Upright stimuli was 81.6 ± 3.7 % and for Inverted stimuli 85.3 ± 6.7 %. In chronic ScZ-patients, HR for Upright stimuli was 73.8 ± 4.4% and for Inverted stimuli 82.5 ± 6.4 %. HR for Upright stimuli was significantly lower for the ScZ than for the control group ($p < 0.05$, 1-way ANOVA followed by *post hoc t*-tests with Bonferroni correction; Fig 2B). For both ScZ and controls, reaction times (RTs) were shorter for upright (0.64 ± 0.04 s and 0.59 ± 0.04 s, respectively for ScZ and controls) than Inverted Mooney-stimuli (0.77 ± 0.09 s and 0.83 ± 0.1 s) (1-way ANOVA followed by *post hoc t*-tests with Bonferroni correction) (Fig 2B).

*Local gamma band oscillations are reduced in chronic ScZ*

In our previous study, we observed reduced local gamma amplitudes in ScZ patients in the current task using sensor time-frequency representations (TFR)-estimates (Grutzner et al., 2013). To confirm these observations with a source-level analysis, we analyzed amplitude modulations across frequency bands separately for both healthy control and ScZ groups. These data were summarized as TFRs which show the fraction of brain areas, parcels, in which the modulation of oscillation amplitudes was statistically significant (Wilcoxon signed rank test, $p < 0.05$ FDR corrected) compared to the prestimulus period. In line with previous observations at the sensor-level (Grutzner et al., 2013), we observed an early amplitude modulation in both low-γ (30–51 Hz) and high-γ (60–120 Hz) bands, which was stronger for the controls than for the ScZ-patients during the post-stimulus period for both upright and inverted stimuli (Fig. 3A) (Welch-test, $p < 0.05$, corrected). We then identified the cortical sources that showed the strongest reduction of high gamma band oscillations in ScZ-patients compared to the control group separately for upright and inverted conditions. We observed reduced gamma oscillations in ScZ-patients for both stimulus conditions in occipital cortex in superior occipital gyrus and sulcus (sOG/S) as well as superior and middle occipital gyri and sulci (s/mOG and s/mOS) but also in intraparietal sulcus (intPS). For the upright

374 condition, ScZ-related reduction in gamma oscillations was also in the temporoparietal junction
375 (TPJ) and superior precentral sulci (sprCS, corresponding to the frontal eye fields, FEF) as well as
376 in middle frontal gyrus (mFG) of the lateral prefrontal cortex (lPFC) (Fig. 3B).

377 Inter-areal synchronization in the lower frequencies from delta to alpha bands may be confounded
378 by stimulus locked phase-synchronization due to the evoked responses (ERs) (Palva and Palva,
379 2012). We therefore also computed the strength of ERs compared to baseline for both conditions
380 and for both groups as well as the difference in the strength of ERs between the groups. These data
381 were then visualized as the fraction of parcels where the modulation of oscillation amplitudes was
382 statistically significant (Wilcoxon signed rank test, $p < 0.05$, FDR corrected) (Fig. 4A). For both
383 upright and inverted conditions, ERs were indeed significantly stronger in controls than in ScZ
384 patients.

385

386 *Inter-areal phase synchrony differs between Controls and ScZ-patients*

387 Our main aim was to investigate whether large-scale synchronization would reveal dysconnectivity
388 anomalies in ScZ-patients. To this end, we quantified stimulus-induced inter-areal phase
389 synchronization between all cortical parcels with the imaginary part of the phase-locking value
390 (iPLV) and to exclude the possible contribution of stimulus evoked activity and synchronization
391 (See Fig. 4A), compared these synchronization estimates against those obtained with forward-
392 inverse-modeled surrogate data (See Methods). We used graph theoretical notation (Bullmore and
393 Sporns, 2009; Rubinov and Sporns, 2010) to visualize inter-areal synchrony so that significant
394 connections were represented as edges and parcels as nodes. As with the oscillation amplitude data,
395 we summarized inter-areal synchronization data using TFRs to indicate the proportion of significant
396 connections from all possible connections (connection density, *K*).

Controls had stronger phase-synchronization compared to ScZ-patients in several frequency bands and at different epochs after stimulus onset for both upright and inverted stimuli: in the theta- (θ, 4–8 Hz) and alpha (α, 8–12 Hz) frequency bands between 0 to 400 ms from stimulus onset and in the low-beta (low-β, 14–20 Hz) and low-γ (30–40 Hz) at around 350 ms (Welch-test, $p < 0.05$ FDR corrected) (Fig. 4B). In addition, for the inverted stimuli we observed weaker synchronization for controls compared to ScZ-patients in between 40–51 Hz. Importantly, these differences in large-scale synchronization remained significant after removing correlations present in the surrogate data and those exhibiting zero-phase-lag synchronization. However, synchronization in the theta band was observed at the same latency window than visual ERs and amplitude modulation (Palva et al., 2011) (See Figure 2A). Accordingly, theta band synchronization likely reflects evoked activity rather than true induced phase-synchronization.

*Long-range gamma-band synchronization connects the nodes in the visual system and frontoparietal network*

To identify group differences in the anatomical layout of synchronization networks in the low-γ frequency (30–40 Hz) band, we identified the most central inter-areal connections and the key cortical areas, *i.e.*, the network hubs (See Methods). For both the upright and inverted conditions, low-γ band synchronization was increased for controls compared to ScZ-patients between left and right-hemispheric visual cortices, specifically between visual areas V1/V2 and several nodes in the lateral occipital cortex (LOC) in both hemispheres including fusiform gyrus (Fus) (Fig. 5). Importantly, V1/V2 and LOC were also strongly connected to inferior frontal sulcus /gyrus (iFS/G) of the lateral prefrontal cortex (lPFC) and intraparietal sulcus (intPS) of the posterior parietal cortex (PPC). These regions belong to dorsal (DAN) and frontoparietal (FPN) attention networks.

Importantly, the fusiform gyrus was a hub in the gamma-band networks only in the upright condition compared to inverted Mooney faces.

*Gamma-band synchronization is correlated with perceptual organization only in controls but not in ScZ-patients*

As ScZ is associated with deficits in the integration of visual features into coherent object representations (Uhlhaas and Mishara, 2007), we also investigated the specific networks underlying perceptual organization through comparing differences in inter-areal synchronization between upright and inverted stimuli in the two groups. Controls showed increased mid-γ band synchronization (40–51 Hz) for upright compared to inverted conditions between 300-400 ms, whereas this increase was absent in ScZ-patients (Fig. 6A). This differential modulation of phase-synchronization was significantly different between control and ScZ groups (Welch's *t*-test, $p < 0.05$, corrected) (Fig. 6B) and involved phase-synchronization patterns between early visual areas V1/V2 and ventral stream (mFG/iFG) of the lPFC) (Fig. 6C). In addition, we observed transiently stronger synchronization for upright than inverted stimuli in the θ-band but this increase in the theta band did not differ significantly between controls and ScZ patients (Fig. 6A).

*Long-range synchronization impairments in ScZ-patients*

We further asked whether the inter-areal mid-γ band synchronization in the upright-inverted perceptual contrast, which was suppressed in ScZ patients, involved long- or short-range connectivity (see Fig. 6). We estimated the parcel-parcel distances of 300 most significant connections and estimated the proportion of these connections in five equiprobable distance bins obtained with parcel-shuffled surrogate data. This analysis showed that the suppression of gamma-

band synchronization in ScZ-patients was most pronounced over medium and long distances (3$^{th}$ and 4$^{th}$ bins) (Fig. 7A).

*The strength of gamma synchronization is correlated with the severity of clinical symptoms of ScZ*

In our previous study (Grutzner et al., 2013), gamma-band oscillation amplitudes were correlated with the severity of the PANSS "disorganization" factor. We thus established whether the changes in perceptual (upright-inverted) mid-γ band (40-51 Hz) synchronization were also linked to clinical features of ScZ. We first estimated graph strength (*GS*) of the mid-γ-band networks in which synchronization was stronger for the upright than inverted trials in controls but not in ScZ patients (See Fig. 6 and Methods). We then estimated the correlation of individual *GS* values with clinical and neuropsychological scores. We found that *GS* in the 40–51 Hz range was negatively correlated with PANSS ($r$ = -0.58, $p$ < 0.03) but not with neuropsychological scores ($r$ = 0.13, $p$ = 0.65) scores (Fig. 7B). The correlation of *GS* with PANSS scores was significant and robust also when estimated with a randomization test (95 % range for shuffled data: $r_{shuffled\ 2.5\%}$ = -0.52 and $r_{shuffled\ 97.5\%}$ = 0.52) and with bootstrapped confidence limits of the correlation coefficient *per se* (95% confidence limits $r_{bootstrap\ 2.5\%}$ = -0.19 and $r_{bootstrap\ 97.5\%}$ = -0.78), respectively.

## Discussion

Impaired cognitive and perceptual functions are a core aspect of ScZ (Green, 1996) but the neuronal mechanisms underlying these deficits are still unclear. One candidate mechanisms is an impairment in the synchronization of oscillatory activity between brain regions (Uhlhaas and Singer, 2010). This perspective is consistent with both current and historical perspectives that have highlighted a disconnection syndrome, a failure in the functional integration of distributed neuronal activity, as a fundamental aspect of the disorder (Friston and Frith, 1995; Stephan et al., 2009).

In the present study, we applied advanced MEG methods for the analyses of local and inter-areal neuronal synchronization as well as graph theoretical measures for the assessment of the large-scale network structures to address this question. The results show that both local synchronization, as reflected in amplitude modulations, and large-scale gamma-band synchronization are reduced in ScZ-patients during a cognitive task requiring perceptual integration. This is in agreement with accumulating evidence that the synchronization of high-frequency oscillations is closely related to perceptual processes and higher cognitive functions during normal brain functions (Kim et al., 2016; Michalareas et al., 2016), the disturbance of which could lead to cognitive and perceptual deficits in ScZ. This is consistent with a large body of evidence that has emerged over recent years that changes in excitatory and inhibitory transmission, in particular deficits in parvalbumin-expressing (PV+) interneurons and *N*-methyl-D-aspartate (NMDA) receptors, constitute a key aspect of cellular abnormalities in ScZ that could give rise to impaired high-frequency oscillations and their synchronization (Gonzalez-Burgos and Lewis, 2012; Kantrowitz and Javitt, 2010; Lewis et al., 2012).

The present study provides critical evidence for a dysfunction in large-scale synchronization in ScZ through the combination of advanced methods of source localization and time series analysis of MEG-data that allow novel insights into the anatomical layout of phase-synchronization abnormalities in ScZ. Specifically, our findings show that abnormal long-range synchronization may constitute a core systems-level mechanism for the cognitive and perceptual deficits in ScZ. In

line with earlier studies on visual perception (Grutzner et al., 2013; Spencer et al., 2008), we observed reduced gamma-band amplitudes in ScZ patients in temporal, posterior parietal (PPC) and lateral prefrontal (PFC) cortices for the upright condition and also in early visual cortices for inverted Mooney faces. This suggests that reductions in high-frequency activity in ScZ-patients are mainly caused by deficits at later stages of the visual hierarchy, which would be in agreement with the evidence that perceptual closure involves higher visual areas (Grutzner et al., 2010) that exert top-down control of visual information processing (Buschman and Kastner, 2015; Corbetta and Shulman, 2002; Corbetta and Shulman, 2011; Womelsdorf and Everling, 2015).

Previous studies have already provided preliminary evidence that long-range synchronization of rhythmic activity could be impaired in ScZ (Spencer et al., 2003; Uhlhaas et al., 2006). However, for the reasons summarized above, these findings are to be interpreted with caution because of the challenges in excluding the confounding factors such as volume conduction, non-neuronal artifacts, and lack of source identification (Palva and Palva, 2012; Schoffelen and Gross, 2009). The present study revealed also a reduction of phase-synchronization for low-frequency oscillations (theta, alpha) in ScZ-patients. As the occurrence of theta-band synchronization overlapped with amplitude and phase-modulation of evoked activity, it is conceivable that these deficits in ScZ-patients may not reflect impairments in genuine large-scale synchronization (Palva and Palva, 2012).

In contrast, synchronization at high gamma frequencies and their reduction in ScZ patients were transient and reflect true induced phase-synchronization patterns which is supported by the analysis of surrogate date. Thus, it appears that both the temporal parsing of evoked responses and the long-range synchronization of these responses are impaired in ScZ patients. Whether the two alterations have a common cause or result from disturbances of different mechanisms is unclear. Support for the specific role of large-scale synchronization at gamma-band frequencies in perceptual organization comes from the comparison of responses to upright vs. inverted Mooney faces. Confirming previous data that suggested a specific role of gamma-band oscillations in the

515 construction of coherent object representations (Grutzner et al., 2013; Honkanen et al., 2015;
516 Morgan et al., 2011; Singer, 1999; Tallon-Baudry and Bertrand, 1999), we observed that controls
517 exhibited a significant, transient increase in phase-synchronization in the mid-gamma-band range
518 (40–50 Hz) at 300–400 ms, which was strongly reduced in ScZ-patients. This reduction comprised
519 interactions both within the visual system, *e.g.*, among early visual regions and fusiform gyrus that
520 underlie face perception (Haxby et al., 2002), as well as between the visual system and key areas of
521 the fronto-parietal and dorsal attention networks in the PPC and lPFC that are involved in the
522 coordination of visual attention (Corbetta and Shulman, 2002; Fox et al., 2005).

523 Moreover, our analyses revealed that reductions in gamma-band synchronization in ScZ-patients
524 involved preferentially medium- and long-distance connections, providing support for the notion
525 that the disorder is associated with impairments in the temporal coordination of distributed neural
526 activity at global scales. Moreover, impairments of temporal coordination were correlated with the
527 severity of the clinical symptoms, supporting the potential relevance of coordination failures in the
528 emergence of clinical symptoms. Taken together, the present study, although not providing causal
529 evidence, yields robust correlative support for the hypothesis that clinical symptoms and cognitive
530 impairments in schizophrenia are associated with a disconnection syndrome (Friston, 1998; Uhlhaas
531 and Singer, 2012; Uhlhaas and Singer, 2015; Voytek and Knight, 2015).

532

533 *Future directions and limitations of the study*

534 We observed reduced γ-band synchronization in chronic ScZ-patients that were under antipsychotic
535 medication. This could potentially constitute a confound for alterations in large-scale
536 synchronization in the disorder. However, we have previously shown that reductions in high-
537 frequency oscillations are present also in unmedicated, first-episode ScZ-patients (Sun et al., 2013)
538 suggesting that antipsychotic medication is not related to alterations in high-frequency activity.

539 Furthermore, preliminary evidence suggests that alterations may be present prior to illness-onset in
540 at-risk individuals (Tada et al., 2016). Future studies are required to determine whether
541 abnormalities in large-scale phase-synchronization predate the onset of frank psychosis and, as a
542 result, could serve as a biomarker for early detection and diagnosis.

543 Additionally, the number of ScZ-patients that entered the analysis is relatively small and replication
544 in larger ScZ-samples is required. The differences observed in phase synchronization between
545 groups, however, were obtained using a conservative data-driven statistical analysis approach and
546 statistical observations were corrected for multiple comparisons. Accordingly, we are confident that
547 the patterns of aberrant synchronization in the current dataset are robust indexes of dysfunctional
548 large-scale networks in ScZ.

549

550 **References**

551 Bell AJ, Sejnowski TJ (1995) An information-maximization approach to blind separation and blind
552 deconvolution. Neural Comput 7:1129-1159.

553 Brookes MJ, Woolrich MW, Barnes GR (2012) Measuring functional connectivity in MEG: A
554 multivariate approach insensitive to linear source leakage. Neuroimage 63:910-920.

555 Bullmore E, Sporns O (2009) Complex brain networks: Graph theoretical analysis of structural and
556 functional systems. Nat Rev Neurosci 10:186-198.

557 Buschman T, Kastner S (2015) From behavior to neural dynamics: An integrated theory of attention.
558 Neuron 88:127-144.

559 Corbetta M, Shulman GL (2002) Control of goal-directed and stimulus-driven attention in the brain.
560 Nat Rev Neurosci 3:201-215.

561 Corbetta M, Shulman GL (2011) Spatial neglect and attention networks. Annu Rev Neurosci
562 34:569-599.

563 Dale A, Sereno M (1993) Improved localization of cortical activity by combining EEG and MEG
564 with MRI cortical surface reconstruction: A linear approach. Journal of Cognitive Neuroscience
565 5:162-176.

566 Dale AM, Liu AK, Fischl BR, Buckner RL, Belliveau JW, Lewine JD, Halgren E (2000) Dynamic
567 statistical parametric mapping: Combining fMRI and MEG for high-resolution imaging of cortical
568 activity. Neuron 26:55-67.

569 Destrieux C, Fischl B, Dale A, Halgren E (2010) Automatic parcellation of human cortical gyri and
570 sulci using standard anatomical nomenclature. Neuroimage 53:1-15.

571 Fox MD, Snyder AZ, Vincent JL, Corbetta M, Van Essen DC, Raichle ME (2005) The human brain
572 is intrinsically organized into dynamic, anticorrelated functional networks. Proc Natl Acad Sci U S
573 A 102:9673-9678.

574 Fries P (2015) Rhythms for cognition: Communication through coherence. Neuron 88:220-235.

575 Friston KJ (1998) The disconnection hypothesis. Schizophr Res 30:115-125.

576 Friston KJ, Frith CD (1995) Schizophrenia: A disconnection syndrome? Clin Neurosci 3:89-97.

577 Gonzalez-Burgos G, Lewis DA (2012) NMDA receptor hypofunction, parvalbumin-positive
578 neurons, and cortical gamma oscillations in schizophrenia. Schizophr Bull 38:950-957.

579 Gramfort A, Luessi M, Larson E, Engemann DA, Strohmeier D, Brodbeck C, Parkkonen L,
580 Hämäläinen MS (2014) MNE software for processing MEG and EEG data. Neuroimage 86:446-460.

581 Green MF (1996) What are the functional consequences of neurocognitive deficits in schizophrenia?
582 Am J Psychiatry 153:321-330.

583 Gregoriou GG, Gotts SJ, Zhou H, Desimone R (2009) Long-range neural coupling through
584 synchronization with attention. Prog Brain Res 176:35-45.

585 Grent-'t-Jong T, Rivolta D, Sauer A, Grube M, Singer W, Wibral M, Uhlhaas PJ (2016) MEG-
586 measured visually induced gamma-band oscillations in chronic schizophrenia: Evidence for
587 impaired generation of rhythmic activity in ventral stream regions. Schizophr Res 176:177-185.

588 Grutzner C, Uhlhaas PJ, Genc E, Kohler A, Singer W, Wibral M (2010) Neuroelectromagnetic
589 correlates of perceptual closure processes. J Neurosci 30:8342-8352.

590 Grutzner C, Wibral M, Sun L, Rivolta D, Singer W, Maurer K, Uhlhaas PJ (2013) Deficits in high-
591 (>60 hz) gamma-band oscillations during visual processing in schizophrenia. Front Hum Neurosci
592 7:88.

593 Hämäläinen MS, Ilmoniemi RJ (1994) Interpreting magnetic fields of the brain: Minimum norm
594 estimates. Med Biol Eng Comput 32:35-42.

595 Haxby JV, Hoffman EA, Gobbini MI (2002) Human neural systems for face recognition and social
596 communication. Biol Psychiatry 51:59-67.

597 Honkanen R, Rouhinen S, Wang SH, Palva JM, Palva S (2015) Gamma oscillations underlie the
598 maintenance of feature-specific information and the contents of visual working memory. Cereb
599 Cortex 25:3788-3801.

600 Kantrowitz JT, Javitt DC (2010) N-methyl-d-aspartate (NMDA) receptor dysfunction or
601 dysregulation: The final common pathway on the road to schizophrenia? Brain Res Bull 83:108-121.

602 Kay SR, Fiszbein A, Opler LA (1987) The positive and negative syndrome scale (PANSS) for
603 schizophrenia. Schizophr Bull 13:261-276.

604 Keefe RS, Goldberg TE, Harvey PD, Gold JM, Poe MP, Coughenour L (2004) The brief
605 assessment of cognition in schizophrenia: Reliability, sensitivity, and comparison with a standard
606 neurocognitive battery. Schizophr Res 68:283-297.

607 Keil A, Muller MM, Ray WJ, Gruber T, Elbert T (1999) Human gamma band activity and
608 perception of a gestalt. J Neurosci 19:7152-7161.

609 Kim H, Ahrlund-Richter S, Wang X, Deisseroth K, Carlen M (2016) Prefrontal parvalbumin
610 neurons in control of attention. Cell 164:208-218.

611 Korhonen O, Palva S, Palva JM (2014) Sparse weightings for collapsing inverse solutions to
612 cortical parcellations optimize M/EEG source reconstruction accuracy. J Neurosci Methods
613 226C:147-160.

614 Lachaux JP, Rodriguez E, Martinerie J, Varela FJ (1999) Measuring phase synchrony in brain
615 signals. Hum Brain Mapp 8:194-208.

616 Lewis DA, Curley AA, Glausier JR, Volk DW (2012) Cortical parvalbumin interneurons and
617 cognitive dysfunction in schizophrenia. Trends Neurosci 35:57-67.

618 Lin FH, Belliveau JW, Dale AM, Hämäläinen MS (2006) Distributed current estimates using
619 cortical orientation constraints. Hum Brain Mapp 27:1-13.

620 Lindenmayer JP, Grochowski S, Hyman RB (1995) Five factor model of schizophrenia: Replication
621 across samples. Schizophr Res 14:229-234.

622 Michalareas G, Vezoli J, van Pelt S, Schoffelen J, Kennedy H, Fries P (2016) Alpha-beta and
623 gamma rhythms subserve feedback and feedforward influences among human visual cortical areas.
624 Neuron .

625 Mooney CM, Ferguson GA (1951) A new closure test. Can J Psychol 5:129-133.

626 Morgan HM, Muthukumaraswamy SD, Hibbs CS, Shapiro KL, Bracewell RM, Singh KD, Linden
627 DE (2011) Feature integration in visual working memory: Parietal gamma activity is related to
628 cognitive coordination. J Neurophysiol 106:3185-3194.

629 Muthukumaraswamy SD, Singh KD (2013) Visual gamma oscillations: The effects of stimulus type,
630 visual field coverage and stimulus motion on MEG and EEG recordings. Neuroimage 69:223-230.

631 Nolte G, Bai O, Wheaton L, Mari Z, Vorbach S, Hallett M (2004) Identifying true brain interaction
632 from EEG data using the imaginary part of coherency. Clin Neurophysiol 115:2292-2307.

633 Palva JM, Monto S, Kulashekhar S, Palva S (2010) Neuronal synchrony reveals working memory
634 networks and predicts individual memory capacity. Proc Natl Acad Sci U S A 107:7580-7585.

635 Palva JM, Zhigalov A, Hirvonen J, Korhonen O, Linkenkaer-Hansen K, Palva S (2013) Neuronal
636 long-range temporal correlations and avalanche dynamics are correlated with behavioral scaling
637 laws. Proc Natl Acad Sci U S A 110:3585-3590.

638 Palva S, Palva JM (2012) Discovering oscillatory interaction networks with M/EEG: Challenges
639 and breakthroughs. Trends Cogn Sci 16:219-230.

640 Palva S, Linkenkaer-Hansen K, Naatanen R, Palva JM (2005) Early neural correlates of conscious
641 somatosensory perception. J Neurosci 25:5248-5258.

642 Palva S, Kulashekhar S, Hamalainen M, Palva JM (2011) Localization of cortical phase and
643 amplitude dynamics during visual working memory encoding and retention. J Neurosci 31:5013-
644 5025.

645 Rodriguez E, George N, Lachaux JP, Martinerie J, Renault B, Varela FJ (1999) Perception's shadow:
646 Long-distance synchronization of human brain activity. Nature 397:430-433.

647 Rouhinen S, Panula J, Palva JM, Palva S (2013) Load dependence of beta and gamma oscillations
648 predicts individual capacity of visual attention. J Neurosci 33:19023-19033.

649 Rubinov M, Sporns O (2010) Complex network measures of brain connectivity: Uses and
650 interpretations. Neuroimage 52:1059-1069.

651 Schoffelen JM, Gross J (2009) Source connectivity analysis with MEG and EEG. Hum Brain Mapp
652 30:1857-1865.

653 Sharon D, Hamalainen MS, Tootell RB, Halgren E, Belliveau JW (2007) The advantage of
654 combining MEG and EEG: Comparison to fMRI in focally stimulated visual cortex. Neuroimage
655 36:1225-1235.

656 Siebenhuhner F, Wang SH, Palva JM, Palva S (2016) Cross-frequency synchronization connects
657 networks of fast and slow oscillations during visual working memory maintenance. Elife
658 5:10.7554/eLife.13451.

659 Singer W (1999) Neuronal synchrony: A versatile code for the definition of relations? Neuron
660 24:49-65, 111-25.

661 Singer W (2009) Distributed processing and temporal codes in neuronal networks. Cogn Neurodyn
662 3:189-196.

663 Spencer KM, Niznikiewicz MA, Shenton ME, McCarley RW (2008) Sensory-evoked gamma
664 oscillations in chronic schizophrenia. Biol Psychiatry 63:744-747.

665 Spencer KM, Nestor PG, Niznikiewicz MA, Salisbury DF, Shenton ME, McCarley RW (2003)
666 Abnormal neural synchrony in schizophrenia. J Neurosci 23:7407-7411.

667 Stephan KE, Friston KJ, Frith CD (2009) Dysconnection in schizophrenia: From abnormal synaptic
668 plasticity to failures of self-monitoring. Schizophr Bull 35:509-527.

669 Sun L, Castellanos N, Grutzner C, Koethe D, Rivolta D, Wibral M, Kranaster L, Singer W, Leweke
670 MF, Uhlhaas PJ (2013) Evidence for dysregulated high-frequency oscillations during sensory
671 processing in medication-naive, first episode schizophrenia. Schizophr Res 150:519-525.

672 Tada M, Nagai T, Kirihara K, Koike S, Suga M, Araki T, Kobayashi T, Kasai K (2016) Differential
673 alterations of auditory gamma oscillatory responses between pre-onset high-risk individuals and
674 first-episode schizophrenia. Cereb Cortex 26:1027-1035.

675 Tallon-Baudry C, Bertrand O (1999) Oscillatory gamma activity in humans and its role in object
676 representation. Trends Cogn Sci 3:151-162.

677 Tallon-Baudry C, Bertrand O, Delpuech C, Pernier J (1996) Stimulus specificity of phase-locked
678 and non-phase-locked 40 hz visual responses in human. J Neurosci 16:4240-4249.

679 Taulu S, Simola J, Kajola M (2005) Applications of the signal space separation method. IEEE Trans
680 Signal Process 53:3359-13.

681 Uhlhaas PJ (2015) Neural dynamics in mental disorders. World Psychiatry 14:116-118.

682 Uhlhaas PJ, Mishara AL (2007) Perceptual anomalies in schizophrenia: Integrating phenomenology
683 and cognitive neuroscience. Schizophr Bull 33:142-156.

684 Uhlhaas PJ, Singer W (2012) Neuronal dynamics and neuropsychiatric disorders: Toward a
685 translational paradigm for dysfunctional large-scale networks. Neuron 75:963-980.

686 Uhlhaas PJ, Singer W (2015) Oscillations and neuronal dynamics in schizophrenia: The search for
687 basic symptoms and translational opportunities. Biol Psychiatry 77:1001-1009.

688 Uhlhaas PJ, Linden DE, Singer W, Haenschel C, Lindner M, Maurer K, Rodriguez E (2006)
689 Dysfunctional long-range coordination of neural activity during gestalt perception in schizophrenia.
690 J Neurosci 26:8168-8175.

691 Varela F, Lachaux JP, Rodriguez E, Martinerie J (2001) The brainweb: Phase synchronization and
692 large-scale integration. Nat Rev Neurosci 2:229-239.

693 Vinck M, Oostenveld R, van Wingerden M, Battaglia F, Pennartz CM (2011) An improved index of
694 phase-synchronization for electrophysiological data in the presence of volume-conduction, noise
695 and sample-size bias. Neuroimage 55:1548-1565.

696 Voytek B, Knight RT (2015) Dynamic network communication as a unifying neural basis for
697 cognition, development, aging, and disease. Biol Psychiatry 77:1089-1097.

698 Weinberger DR, Berman KF, Illowsky BP (1988) Physiological dysfunction of dorsolateral
699 prefrontal cortex in schizophrenia. III. A new cohort and evidence for a monoaminergic mechanism.
700 Arch Gen Psychiatry 45:609-615.

701 Womelsdorf T, Everling S (2015) Long-range attention networks: Circuit motifs underlying
702 endogenously controlled stimulus selection. Trends Neurosci 38:682-700.

703 Yeo BT, Krienen FM, Sepulcre J, Sabuncu MR, Lashkari D, Hollinshead M, Roffman JL, Smoller
704 JW, Zollei L, Polimeni JR, Fischl B, Liu H, Buckner RL (2011) The organization of the human
705 cerebral cortex estimated by intrinsic functional connectivity. J Neurophysiol 106:1125-1165.

706

707

708

## 709 Figure Legends

710 **Table 1**. Means, standard deviations, and mean differences for demographic, neurocognitive, and
711 clinical characteristics of controls and schizophrenia patients.

712

713 **Figure 1.** A schematic overview of the analysis pipeline showing the different analysis steps and
714 outputs of the results (for a-s, see Methods).

715

716 **Figure 2. Stimuli and behavioural performance in ScZ-patients and Controls.** (A) Upright (top)
717 and inverted (Bottom) Mooney face stimuli used in the task. (B) Hit rates (HR) and reaction times
718 (RTs) for both groups for the upright and inverted stimuli. Lines indicate significant difference
719 between the groups (* = $p < 0.01$, 1-way ANOVA, Bonferroni corrected at $\alpha = 0.05/4$).

720

721 **Figure 3**. **Time-frequency representations (TFR) of significant oscillation amplitude**
722 **modulations.** (A) Difference in oscillation amplitudes between controls (CS) and ScZ patients for
723 the correctly perceived upright and inverted stimuli (Welch's *t*-test, $p < 0.05$, corrected). Color-

scale indicates the fraction of brain regions with a significant positive CS-ScZ difference. The fraction of significant negative effects was negligible (blue colors). (B) Cortical regions in which significant differences in oscillation amplitudes between the CS and ScZ were observed for the selected time-frequency (TF) region of interest indicated by rectangles in panel *A* for upright and inverted stimuli displayed on inflated cortical surfaces. Colors of the parcels indicate the fraction of time-frequency (TF) elements with significant modulation in the parcel. Acronyms for the anatomical and function brain areas: FEF, frontal eye fields; iPG, inferior parietal gyrus (here angular gyrus); intPS, intraparietal sulcus; mFS/G, middle frontal sulcus/gyrus; mTS, middle temporal sulcus; poCS, postcentral sulcus, sOS/G, superior occipital sulcus/gyrus; sPG, superior parietal gyrus; sTS, superior temporal sulcus; TPJ, temporoparietal junction; V1/V2, primary/secondary visual cortex.

**Figure 4. Inter-areal stimulus induced synchronization is stronger for the SC than for ScZ.** C) A) The extent of evoked responses across cortical parcels for the upright and inverted stimuli separately for the CS and ScZ subjects. The *y*-axis displays the proportion of cortical regions in which the evoked response was stronger than in baseline (Wilcoxon signed ranked test, $p < 0.05$, FDR corrected). The lines above indicate significant differences between the groups (Welch-test, $p < 0.05$, FDR corrected). B) The extent of significantly different inter-areal synchronization between controls (SC) and ScZ patients. TFRs show synchronization separately for upright and inverted stimuli as estimated with iPLV. Colour-scale indicates the connection density (*K*) *e.g.,* the proportion of statistically significant connections of synchrony from all possible connections between groups (Welch's *t*-test, $p < 0.05$ FDR corrected).

747 **Figure 5. Cortical networks of low-γ synchronization that differ between CS and ScZ.** (A)
748 Low-gamma (low-γ) band networks that were stronger for controls than ScZ subjects for the
749 Upright and Inverted stimuli in the time-frequency (TF) ROI of 30–40 Hz and 150–350 ms. Graphs
750 display 200 strongest connections on an inflated and flattened cortical surface. Colors and
751 abbreviations as in Fig 2. Additional abbreviations: AG, angular gyrus; iFS/G, inferior frontal
752 sulcus/gyrus; MI, primary motor cortex; mOG = middle occipital gyrus; mTG, middle temporal
753 gyrus; Fus, fusiform gyrus; POS, parieto-occipital sulcus; prCN, precuneus; SI, primary
754 somatosensory cortex; sTG, superior temporal gyrus.

755

756 **Figure 6**. **Gamma-band synchronization reflects perceptual binding in CS and is stronger in**
757 **CS than in ScZ. A)** TFR for the difference in the strength of parcel-to-parcel synchronization
758 between correctly perceived upright and inverted trials separately for CS and ScZ as estimated with
759 iPLV (Wilcoxon-tests, $p < 0.05$, FDR corrected). **B)** TFR for the difference between CS and ScZ
760 groups in the upright-inverted contrast (Welch's *t*-test, $p < 0.05$ FDR corrected). Rectangle indicate
761 the ROI selected for visualization in C. **C)** Mid-γ band (40–50 Hz) network that for the upright-
762 inverted contrast that was stronger for CS and ScZ group in the 200–300 ms time window (the
763 graph is displayed as those in Fig. 5, abbreviations as in Fig 3 and 5. CS = central sulcus, iTG =
764 inferior temporal gyrus, SMA = supplementary motor area.

765

766 **Figure 7. The severity of ScZ is correlated with the strength of mid-γ band synchronization.**
767 **Long-range gamma synchronization related to perceptual binding is reduced in ScZ**. **A)** The
768 fractions of significant connections of perceptual (upright-inverted) mid-γ band (40–51 Hz,
769 325–425 ms) synchronization (*y*-axis) divided into five connection-length bins according to their

770 normalized eucledian distance distributions (*x*-axis). The proportion of significant connections in
771 each bin was estimated separately for the 300 of most significant connections and compared to
772 parcel-shuffled surrogates. Black and grey lines indicate the mean and 2 SD of surrogate data. **B)**
773 The correlation of the graph strength (*GS*) with the disorganization PANSS and neuropsychological
774 scores estimated for mid-γ band *GS* (41–50 Hz, 325–425 ms) for the difference between upright
775 and inverted stimuli.

776

777

# Table 1

| | Healthy Controls (N = 19) | | Chronic Patients (N = 16) | | Statistics | |
|---|---|---|---|---|---|---|
| **Basics** | Mean | SD | Mean | SD | $X^2$-/*t*-value | *p*-value |
| Gender (m/f) | 13/6 | | 10/6 | | $X^2_1 = 1.01$ | 0.71 |
| Age | 32.42 | 10.61 | 37.06 | 9.47 | $t_{33} = -1.37$ | 0.18 |
| Education | 15.5 | 3.17 | 13.94 | 3.30 | $t_{31} = 1.16$ | 0.25 |
| Handedness | 76 | 42.06 | 77 | 42.13 | $t_{29} = -0.03$ | 0.97 |
| **BACS** | | | | | | |
| Verbal Memory | 51.61 | 7.06 | 37.87 | 14.40 | $t_{30} = 3.43$ | 0.0018 |
| Digit | 24.56 | 3.99 | 19.53 | 4.41 | $t_{30} = 3.22$ | 0.0031 |
| Motor | 89.65 | 9.03 | 74.87 | 11.09 | $t_{29} = 3.99$ | 0.0004 |
| Fluency | 58.83 | 13.7 | 42.13 | 9.21 | $t_{30} = 2.96$ | 0.0060 |
| Symbol cod. | 55.67 | 14.84 | 46.87 | 15.72 | $t_{30} = 1.57$ | 0.1269 |
| ToL | 19.83 | 2.2 | 18.07 | 2.71 | $t_{30} = 2.07$ | 0.0467 |
| **PANSS** | | | | | | |
| Negative | - | - | 16.6 | 4.76 | - | - |
| Excitement | - | - | 6.07 | 1.83 | - | - |
| Positive | - | - | 9.4 | 3.98 | - | - |
| Cognition | - | - | 9.6 | 3.14 | - | - |
| Depression | - | - | 12.67 | 3.62 | - | - |
| Disorganization | - | - | 5.53 | 2.00 | - | - |
| Total Score | - | - | 238.84 | 43.09 | - | - |

778

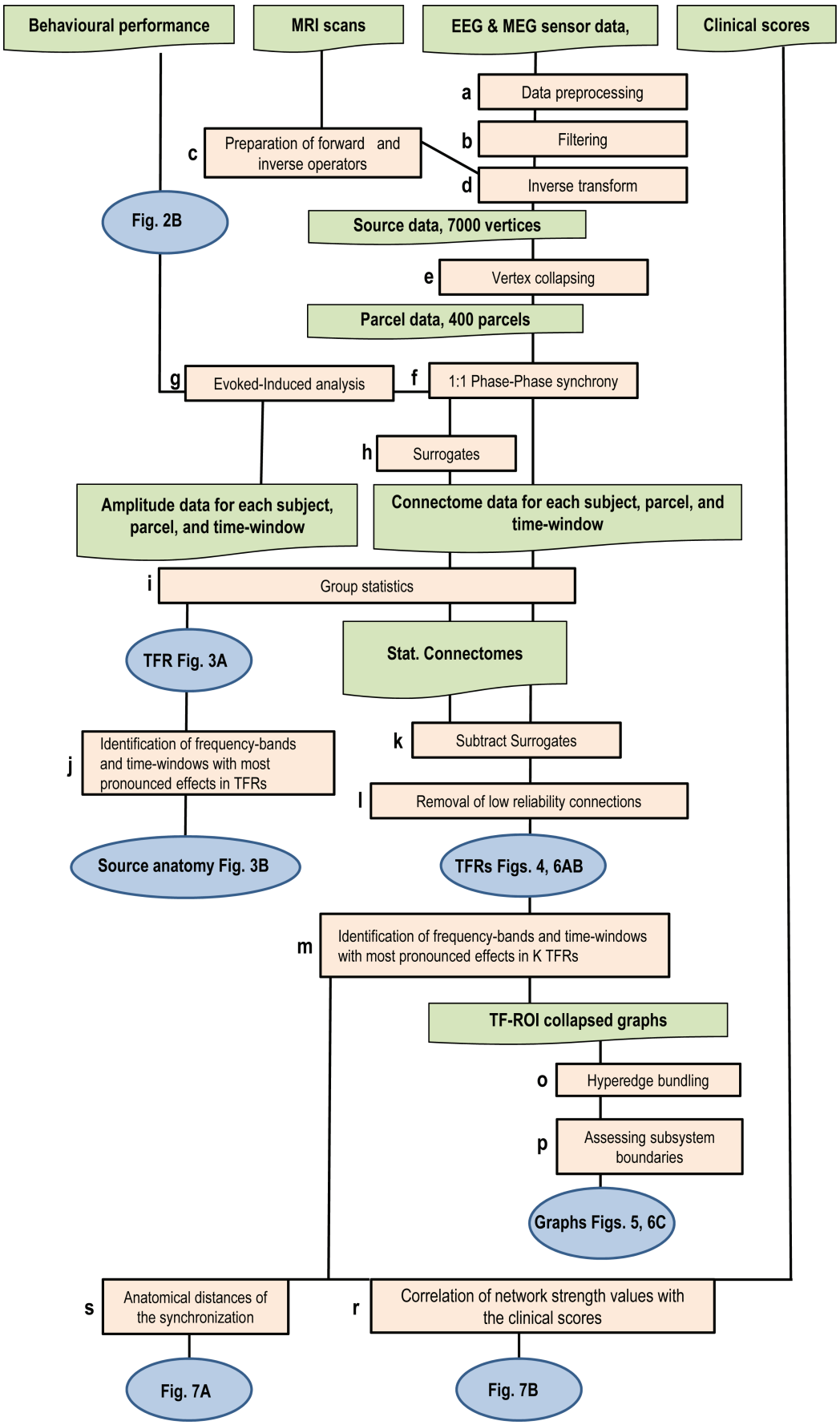

A

B

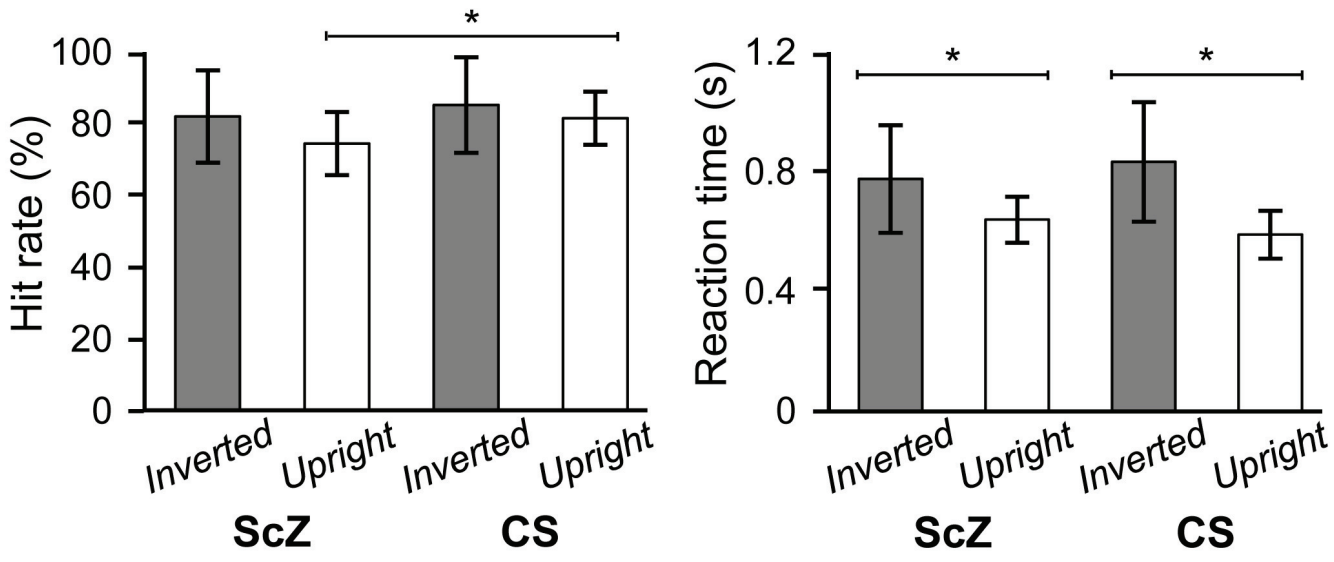

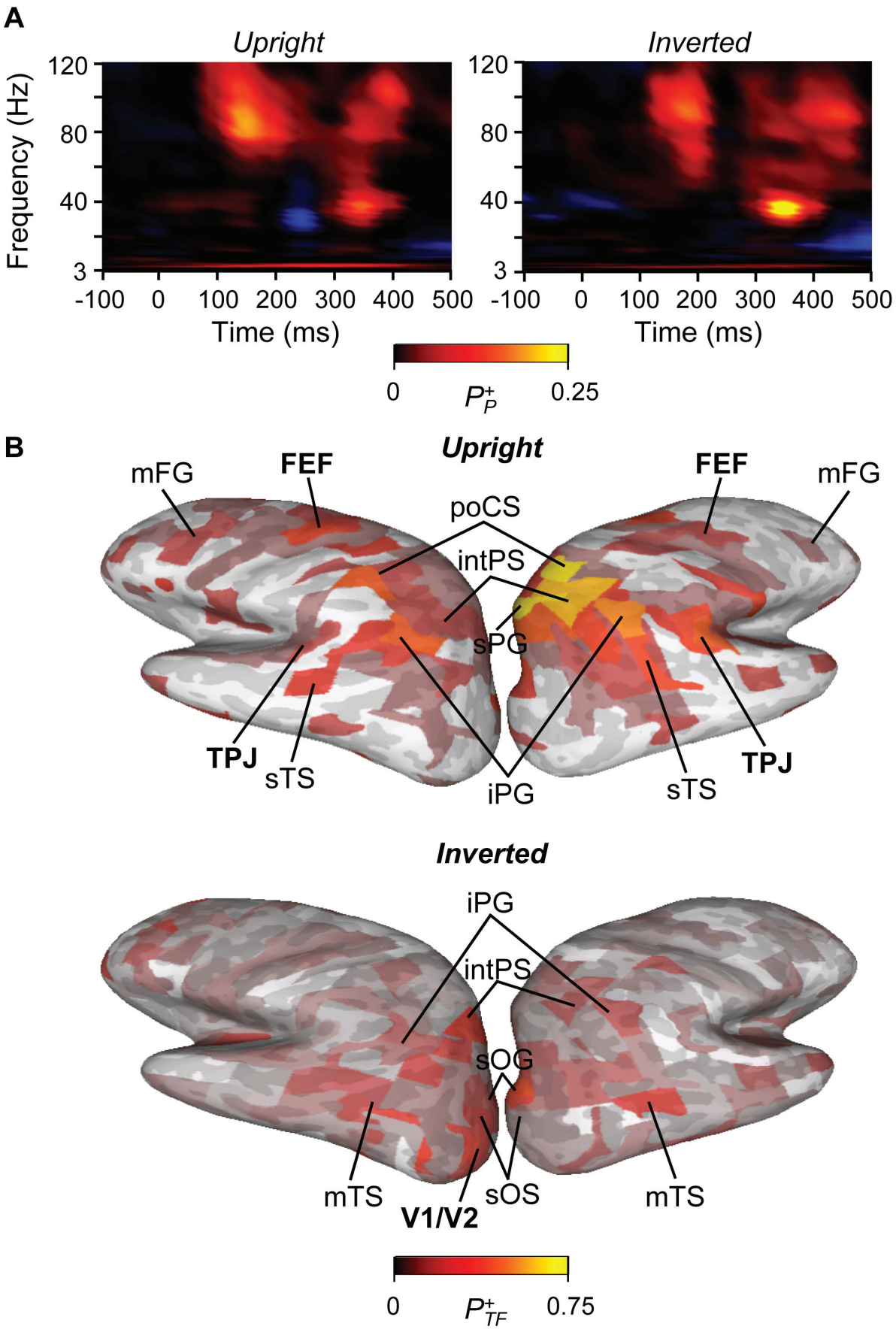

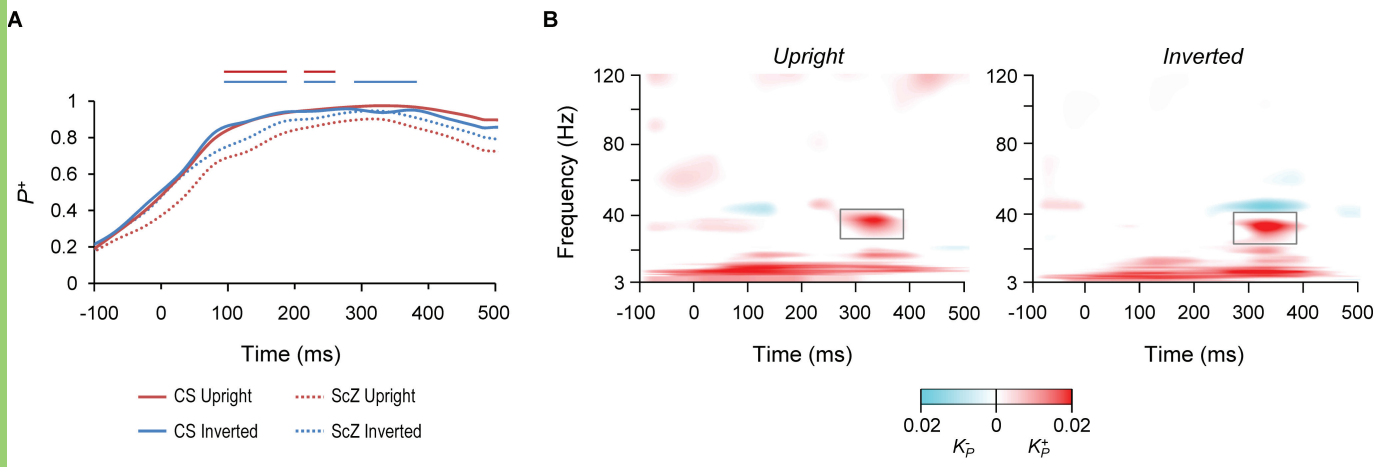

***Upright***

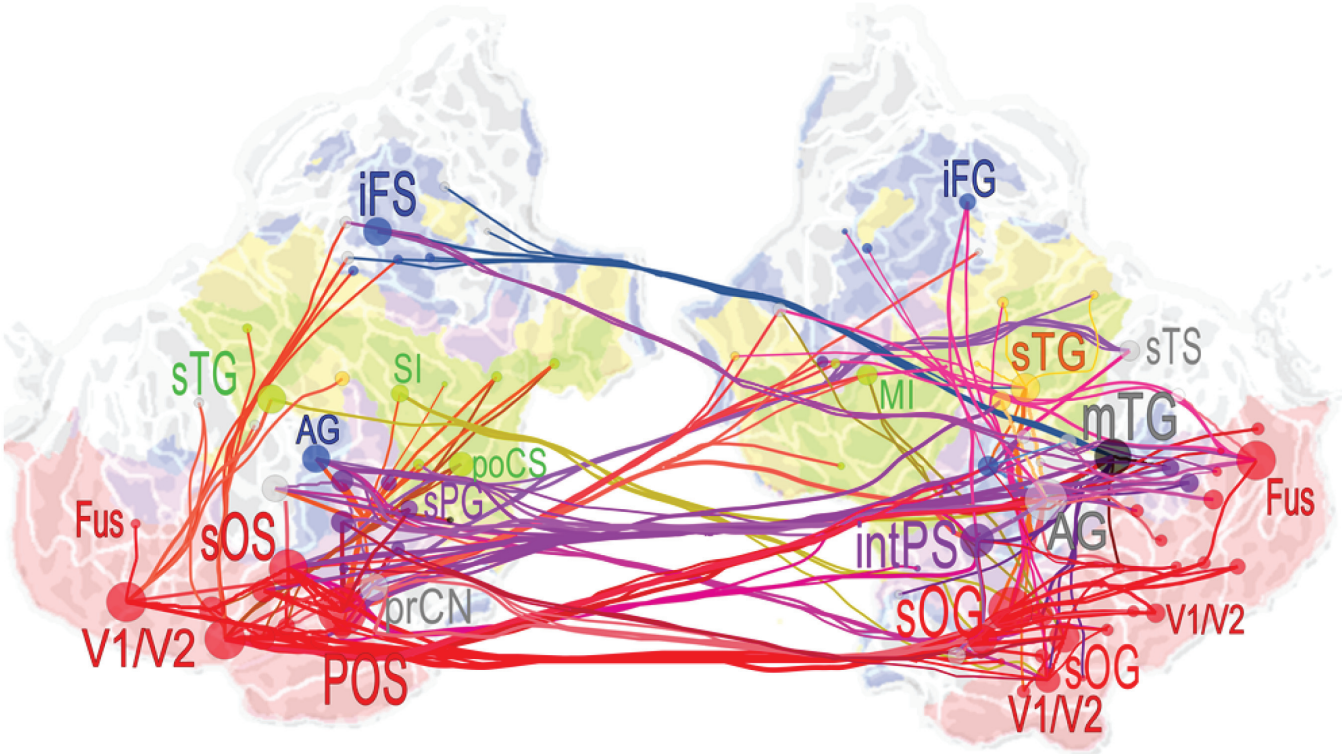


***Inverted***

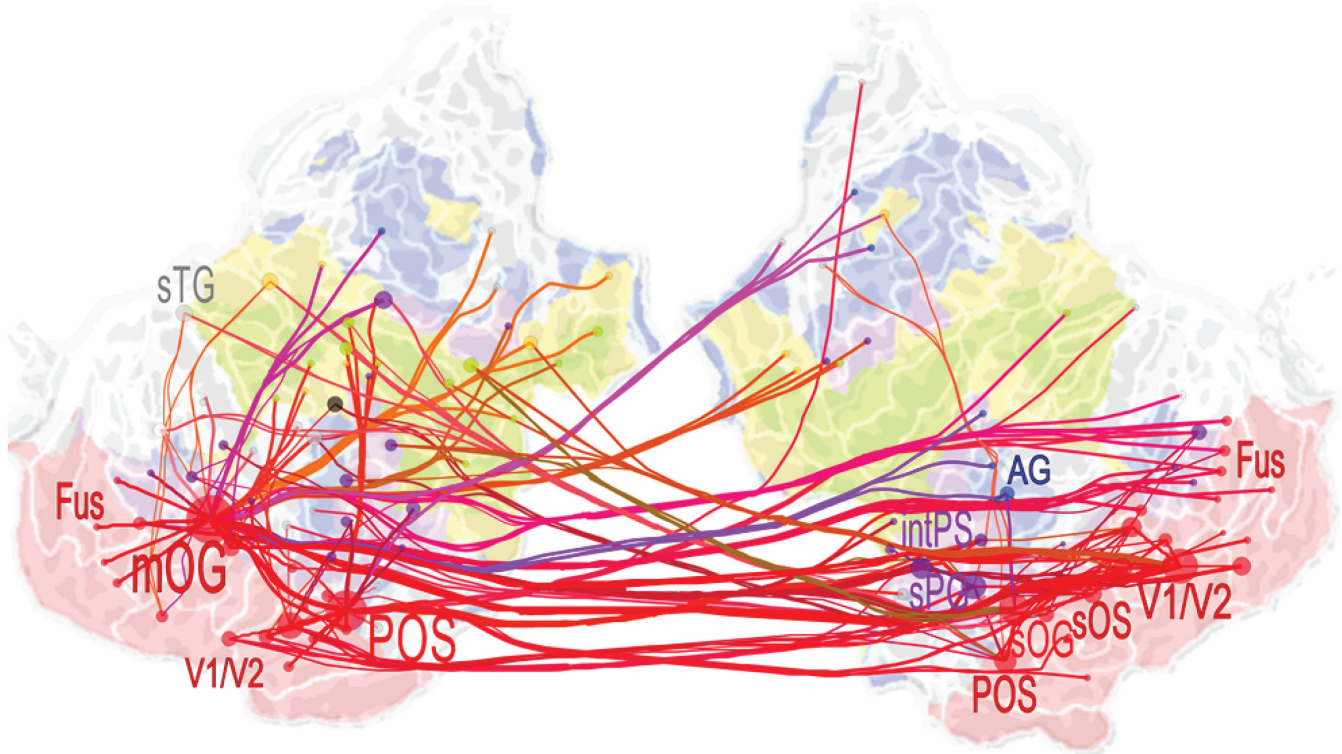


Vis | SM | DAN | VAN | Lim | FP | Def